

Full tunability enabled by Floquet engineering in a multilevel quantum dot system

Yuan Zhou,^{1,2} Sisi Gu,^{1,2} Ke Wang,^{1,2} Gang Cao,^{1,2} Xuedong Hu,³ Ming Gong,^{1,2,*} Guang-Can Guo,^{1,2} Hai-Ou Li,^{1,2,†} and Guo-Ping Guo^{1,2,4,‡}

¹CAS Key Laboratory of Quantum Information, University of Science and Technology of China, Hefei, Anhui 230026, China

²CAS Center for Excellence and Synergetic Innovation Center in Quantum Information and Quantum Physics, University of Science and Technology of China, Hefei, Anhui 230026, China

³Department of Physics, University at Buffalo, SUNY, Buffalo, New York 14260, USA

⁴Origin Quantum Computing Company Limited, Hefei, Anhui 230026, China

(Dated: June 9, 2022)

Tunability of an artificial quantum system is crucial to its capability to process quantum information. However, tunability usually poses significant demand on the design and fabrication of a device. In this work, we demonstrate that Floquet engineering based on longitudinal driving provides distinct possibilities in enhancing the tunability of a quantum system without needing additional resources. In particular, we study a multilevel model based on gate-defined double quantum dots (DQDs) where the Landau-Zener-Stückelberg (LZS) interference could occur. We propose an effective model to describe the LZS interference in this multilevel system, and show that it is highly tunable via the driving field. We then illustrate the versatility and rich physics of a driven multilevel system by exploring phenomena such as Autler-Townes Splitting (ATS), adiabatic state transfer, and dark state. In the context of qubit control, we propose noise-resistant quantum gates based on adiabatic passage. The theoretical consideration we present here is rather general, and is in principle valid for other multilevel quantum systems.

I. INTRODUCTION

Recent developments in quantum coherent devices has pushed the state-of-the-art ever closer to the requirements of fault-tolerant quantum computation [1–10]. Tunability of a quantum system is a crucial ingredient and a capacity enhancer to its applications in quantum information processing. While more tunable usually means additional elements in the device design, and therefore more complex to fabricate, Floquet engineering via a periodic drive [11–14] could help solve this dilemma. This approach has been employed to tailor quantum systems [15–17], and leads to interesting phenomena such as Floquet topological insulators [13, 14]. Applied strategically, Floquet engineering could enable significant tunability while avoiding complex designs. Specifically, under a periodic drive, a qubit is dressed by the photons, and the driving field amplitude and frequency would provide new tuning knobs for the dressed qubit [18–21].

For a two-level system, LZS interference [22–24] is a prominent example of Floquet engineering, with the coherent phase controllable via driving amplitude and frequency. Indeed, LZS interference has been demonstrated in superconducting circuits [25–27], gate-defined DQDs [28–30], and nitrogen-vacancy color centers [31]. LZS interference could occur in a multilevel system as well. One intriguing and potentially attractive feature of a multilevel system is the presence of multiple paths of evolution, leading to higher-order interference that could reveal interesting multilevel physics. Most importantly, coherent

phases in a driven multilevel system remain tunable via driving amplitude and frequency, so that tunability can still be achieved. Such multilevel dynamics is not yet deeply explored in the literature. Some multilevel studies are dominated by two-level dynamics, so that they can be well characterized by effective two-level models [30, 32, 33]. In other cases the results are interpreted by numerical simulations [34], or by treating the anticrossings separately [35], or by introducing additional assumptions [36], which tend to obscure the original physics. An effective model based on high-frequency expansion was developed [37–39], though we would show that it fails to capture the multilevel dynamics studied here. In short, theoretical understanding of a driven multilevel system with driving frequency similar to energy splittings is still lacking [24].

Gate-defined quantum dots (QD) provide a viable platform for quantum computation and quantum simulation, having advantages such as high degree of integration, all-electrical control, and potentially higher operating temperatures [40–42]. With a strong longitudinal drive of broad bandwidth, LZS interference has been widely observed, and applied to qubit manipulation [28], dephasing characterization [30], spectroscopy [29], *etc.* With precise state control and measurement available in QDs, they are also an ideal platform for exploring multilevel LZS interference, and will be the nominal system we will explore in this work.

Here we study a prototype multilevel system under a longitudinal drive, which can be straightforwardly constructed in a gate-defined DQD. We solve this model problem by performing a proper unitary transformation, expanding in the Floquet basis, and then performing a Schrieffer-Wolff transformation. We find that the multilevel LZS dynamics is accurately captured by the result-

* gongm@ustc.edu.cn

† haiouli@ustc.edu.cn

‡ gpguo@ustc.edu.cn

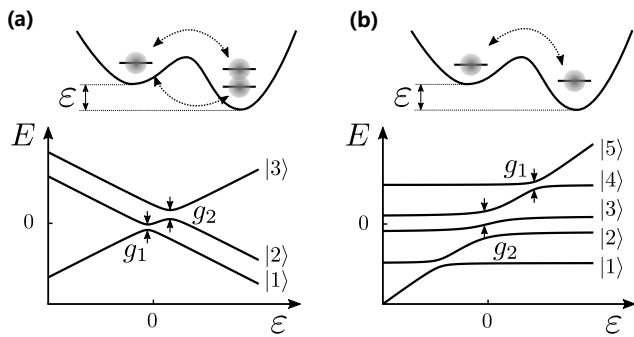


FIG. 1. **Gate-defined QDs and their lowest energy levels.** (a) Realization of the three-level model based on a hybrid qubit with three spins. (b) Realization of the five-level model based on the singlet-triplet qubit system. In these systems, the off-diagonal couplings g_i between different states are realized based on tunneling through the barrier and spin-orbit coupling, while the energies in the diagonal terms can be tuned by the detuning between the two quantum dots, denoted by ε .

ing effective model, where the synthetic couplings are tunable by the driving field. Based on this model, we study multilevel physics under a variety of conditions, and demonstrate several celebrated phenomena that have been observed in atomic and other systems via transverse driving, such as ATS [43–45], electromagnetically induced transparency [46–53], and adiabatic state transfer [48, 54–59]. We investigate these phenomena both numerically and theoretically, with focus on the distinct features due to longitudinal driving. Lastly, we explore applications of the high-order interference in the context of qubit control in a two-spin system. Our proposal reveals intriguing applications of Floquet engineering in general and LZS in particular in quantum computation and quantum simulation, and broadens the prospect of QDs for future quantum coherent devices.

II. MULTILEVEL MODELS AND AN EFFECTIVE HAMILTONIAN

We consider the physics in longitudinally driven multilevel systems shown in Fig. 1 (a) and (b). A three-level system is the minimal prototype to demonstrate higher order interference. One example is the three-spin hybrid qubit [60–63] in an asymmetric Si DQD, as shown in Fig. 1 (a). In the subspace with total spin $S = 1/2$ and $S_z = -1/2$, the lowest three levels can be isolated from the excited manifolds, yielding the following basis [60, 64]

$$\begin{aligned} |1\rangle &= |\downarrow, S\rangle, & |2\rangle &= \sqrt{\frac{1}{3}}|\downarrow, T_0\rangle - \sqrt{\frac{2}{3}}|\uparrow, T_-\rangle, \\ |3\rangle &= |S, \downarrow\rangle, \end{aligned} \quad (1)$$

where $|S\rangle = (|\uparrow\downarrow\rangle - |\downarrow\uparrow\rangle)/\sqrt{2}$, $|T_0\rangle = (|\uparrow\downarrow\rangle + |\downarrow\uparrow\rangle)/\sqrt{2}$ and $|T_-\rangle = |\downarrow\downarrow\rangle$ in $|1\rangle$ and $|2\rangle$ are the singlet and

triplet states in the right dot, while $|S\rangle$ in $|3\rangle$ is in the left dot, giving it a different charge occupation and detuning dependence from $|1\rangle$ and $|2\rangle$.

The Hamiltonian governing the three-level system in Fig. 1 (a) takes the form

$$H(t) = \begin{pmatrix} D_1 & 0 & g_1 \\ 0 & D_2 & g_2 \\ g_1 & g_2 & D_3(t) \end{pmatrix}, \quad (2)$$

where we have set $\hbar = 1$. The driving of this system is through the interdot detuning, $D_3(t) = \varepsilon - A \cos(\omega t)$, and is longitudinal. Both couplings g_1 and g_2 are determined by the inter-dot tunneling (typically about 2 – 5 GHz [62]) and are set as constants in this study.

To solve this problem, we perform unitary transformations to shift the time dependence into the basis states, and search for an effective Hamiltonian that is time-independent. Specifically, we first eliminate the time dependence in the diagonal terms of the Hamiltonian by going to a rotating frame through the rotation $\mathcal{U} = \text{diag}(e^{i(D_2+n\omega)t}, e^{iD_2t}, e^{i\int_0^t d\tau [D_3(\tau)+\delta]})$, where $\delta \equiv D_2 - \varepsilon + N\omega$ is a frequency offset. This offset δ ensures the time-translation symmetry $\tilde{H}(t) = \tilde{H}(t+T)$ in the new basis, and keeps the diagonal terms in the first Brillouin zone of the frequency domain. The Hamiltonian in the rotating frame is given by $\tilde{H}(t) = \mathcal{U}^\dagger H(t) \mathcal{U} - i\mathcal{U}^\dagger \partial_t \mathcal{U}$. We then perform the Floquet expansion [65] on \tilde{H} , followed by a Schrieffer-Wolff (SW) transformation [66]. The details of this procedure are presented in Appendix. A.

The effective time-independent Hamiltonian of our driven three-level system is finally obtained as

$$H_{\text{eff}} = \begin{pmatrix} D_{12} - n\omega + \Delta' & \xi & g_1 J_{N-n} \\ \xi^* & \Delta & g_2 J_N \\ g_1^* J_{N-n} & g_2^* J_N & -\delta - \Delta - \Delta' \end{pmatrix}, \quad (3)$$

where $D_{12} = D_1 - D_2$, $J_k = J_k(\frac{A}{\omega})$ is the first-kind Bessel function of the k -th order, and Δ' , Δ , ξ are corrections from the higher harmonics via the second-order SW transformation (see Appendix. B). This effective Hamiltonian is equivalent to the one obtained by the high-frequency expansion [38] when $D_{12} = n\omega$ and $\varepsilon - D_2 = N\omega$. However, as we will show below and in Appendix C, Eq. (3) is valid in a much broader parameter regime because of the more adaptable transformations involved in its derivation. Hereafter we denote $D_i - \varepsilon$ as D_{i3} (i.e. D_{i3} does not include the driving field, and $D_{3i} = -D_{i3}$).

The effective Hamiltonian shows that the original single longitudinal drive has made both the off-diagonal couplings individually tunable. This wide tunability is highly desirable in a hybrid qubit (and the singlet-triplet qubit we discuss below) since it is challenging to tune g_1 and g_2 individually in practice. Furthermore, a synthetic interaction labeled by ξ is now generated, coupling the dressed qubit states $|1\rangle$ and $|2\rangle$.

The same approach can be applied to derive an effective model for a five-level system with energy spectrum

similar to Fig. 1(b). The five-level structure here has been explored in a singlet-triplet (ST) system in a DQD [8, 9, 67–71], and has recently been employed to demonstrate spin-based two-qubit gates with gate fidelity above 99% [8, 9]. The basis states of the ST system are given by

$$\begin{aligned} |1\rangle &= |\uparrow, \uparrow\rangle, & |2\rangle &= |\uparrow, \downarrow\rangle, & |3\rangle &= |\downarrow, \uparrow\rangle, \\ |4\rangle &= |\downarrow, \downarrow\rangle, & |5\rangle &= |S, 0\rangle. \end{aligned} \quad (4)$$

Here states $|1\rangle$ to $|4\rangle$ have one electron in each dot, while $|5\rangle$ has both electrons in the left dot in Fig. 1(b). In the ST system, the coupling denoted by g_2 (couplings between $|2\rangle$, $|3\rangle$ and $|5\rangle$) is given by spin-conserved interdot tunneling, while g_1 (couplings between $|1\rangle$, $|4\rangle$ and $|5\rangle$) represents spin-flip tunneling enabled by spin-orbit interaction. Neither can be tuned conveniently and reliably. Hereafter, state $|3\rangle$ in Eq. (1) and $|5\rangle$ in Eq. 4 will be termed as the shuttle state. These states respond differently to the gate voltage detuning ε due to their different charge configurations as is shown in Fig. 1, and consequently can be detected electrically.

III. AMPLITUDE SPECTROSCOPY AND AUTLER-TOWNES SPLITTING

In a longitudinally driven system, the state spectrum, especially the various anti-crossings, can be characterized using amplitude spectroscopy [26] with a broad bandwidth instead of the conventional spectroscopic approach of varying the frequency of a monochromatic driving field. Here we first investigate resonant conditions for transitions and modulation of effective couplings by amplitude spectroscopy using our effective Hamiltonian and direct numerical simulation using the original time-dependent Hamiltonian.

In Fig. 2 (a) we present the long-time averaged transition amplitude T_{12} between $|1\rangle$ and $|2\rangle$ (see Appendix A 2) based on Floquet theorem using the original $H(t)$, with $g_1 = 0.1$ GHz, $g_2 = 1$ GHz and $\omega = 4$ GHz. Details in the black dashed box are enlarged in Fig. 2 (b)-(d), where the analytical results from the effective model are presented by green dots, in excellent agreement with the numerical simulation.

According to H_{eff} , resonant transitions happen at

$$\begin{aligned} D_{12} &= n\omega + \mathcal{O}(J_N^2/\omega) \\ D_{13} &= m\omega + \mathcal{O}(J_N^2/\omega) \end{aligned} \quad (5)$$

for the principal resonance and higher harmonics of the two branches, with m and n both integers. This result clearly shows that Rabi oscillation based on higher harmonic resonance is possible (for a more detailed discussion see Appendix D). In addition to the modulated effective couplings, we observe splittings in the signals, such as the two branches around $D_{12} = 0$. The splitting is caused by the coupling between $|2\rangle$ and $|3\rangle$. With $\varepsilon = 0$, the coupling and driving hybridize $|2\rangle$ and $|3\rangle$, so that

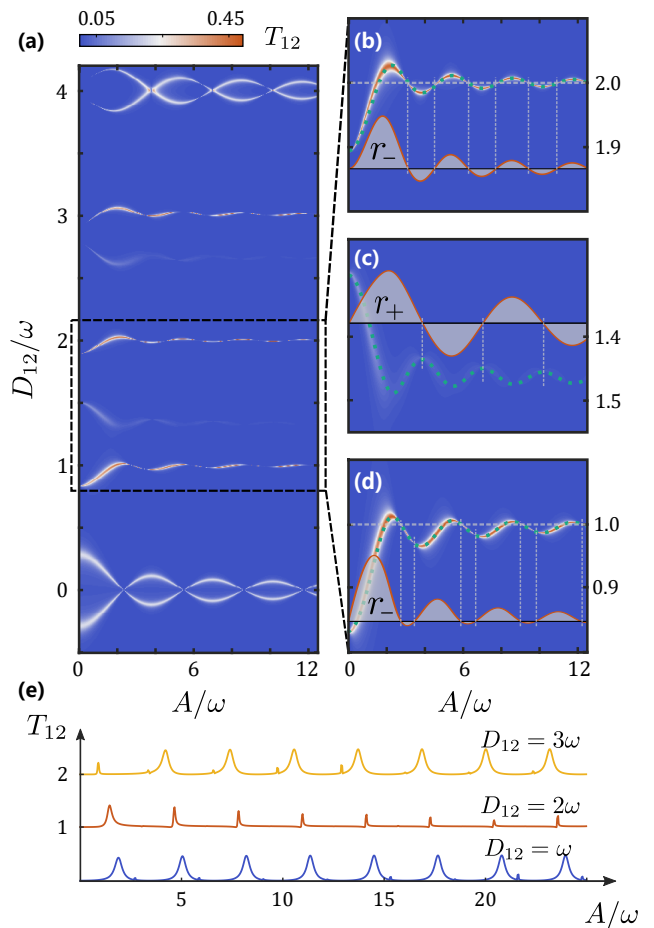


FIG. 2. **The transition amplitude of the driven three-level model.** (a) Time-averaged transition amplitude T_{12} as a function of driving amplitude A and energy spacing D_{12} with parameters $g_1 = 0.1$ GHz, $g_2 = 1$ GHz, $D_1 = -3D_2$ and $\varepsilon = 0$. Significant transition is observed at the resonant condition of Eq. 5. Zoom-in of $D_{12}/\omega \in [0.8, 2.2]$ are placed in (b)-(d), in which the green dotted lines represent the resonance indicated by H_{eff} , and the shaded functions are the effective couplings of r_{\pm} , zero points of which yield the breakpoints. Breakpoints in (b) are well aligned to $D_{12}/\omega = 2$ while those in (d) are not aligned to $D_{12}/\omega = 1$, which is the evidence of odd-even effect. (e) Cross-sections of (a) in $D_{12}/\omega = 1, 2$ and 3 . Signals are shifted for clarity. For $D_{12}/\omega = 2$, the transition is suppressed, and the suppression gets severe as driving amplitude increases.

two absorption peaks develop. Indeed, if we had calculated T_{13} , we would obtain the same patterns as in Fig. 2, just with different intensities, as the system stationary states are all mixtures of $|2\rangle$ and $|3\rangle$. The splittings in the resonant signals for each n -harmonic are an analogue to ATS [43–45]. Different from the original ATS under transverse driving, here the splitting is modulated in the form of $J_N(A/\omega)$ as is shown in Fig. 2 (b)-(d) by the green dotted lines, because the driving here is longitudinal. As the driving amplitude increases into the strong drive $A/\omega \gg 1$ regime, the splitting also saturates.

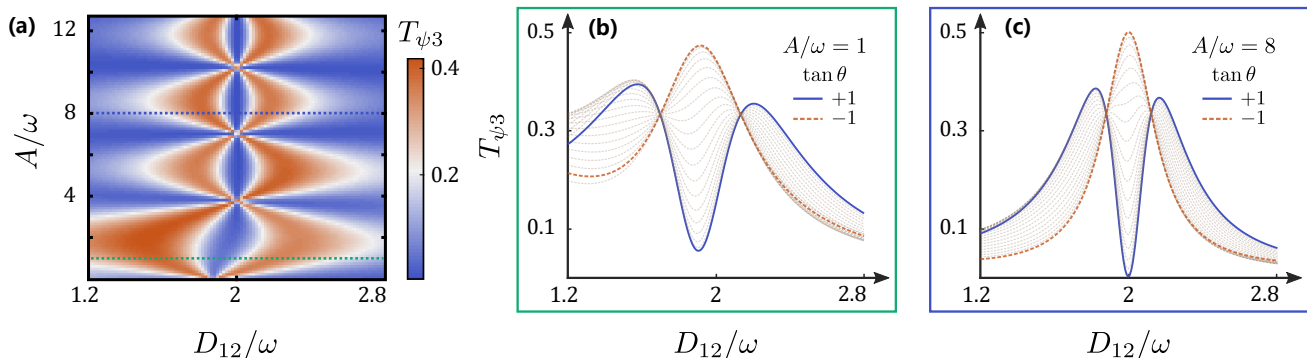


FIG. 3. **Dark state based on the effective three-level model.** (a) Averaged transition amplitude $T_{\psi 3}$ as a function of D_{12} and A , with $D_{12} = 2D_{32}$, $g_1 = g_2 = 1$ GHz, $\omega = 4$ GHz and $\theta = \pi/4$. We focus on the region of $D_{12} \approx 2\omega$ with effective couplings given by $g_1 J_{-1}(A/\omega)$ and $g_2 J_1(A/\omega)$, respectively. As a result, $|\psi(\pi/4)\rangle$ is the dark state in case of $D_{12} = 2\omega$ with ignorable Δ , Δ' and ξ . (b) and (c) show the cross-sections at $A/\omega = 1$ and 8, respectively, with different initial state by scanning the relative phase in $|\psi(\theta)\rangle$. When A/ω is not large enough, the dip will not approach zero due to the tiny contribution of Δ , Δ' and ξ .

Simulation results in Fig. 2 also exhibit other remarkable features. For example, as driving amplitude A increases, we observe break points along the resonant curves where T_{12} vanishes or is strongly suppressed. To understand this feature, we examine more closely the regime where hybridization between $|2\rangle$ and $|3\rangle$ is strong. In order to evaluate the transition amplitude accurately, we first diagonalize the subspace of $\{|2\rangle, |3\rangle\}$ as $\text{diag}(E_+, E_-)$, with the new basis denoted by $\{|+\rangle, |-\rangle\}$. Effective couplings between $|1\rangle$ and $|\pm\rangle$ denoted by r_{\pm} are presented in the inset in Fig. 2 (b)-(d), showing that the break points occur at $r_{\pm} = 0$ exactly. In other words, the break points mean that tunneling between $|1\rangle$ and $|\pm\rangle$ is forbidden, similar to the coherent destruction of tunneling in a driven two-level system [25, 29, 72], though extended to a multilevel system here.

The coherent destruction of tunneling leads to a striking odd-even alternating effect. In Fig. 2 (b) the break-points are well aligned to $D_{12}/\omega = 2$ while the distribution of the breakpoints in Fig. 2 (d) are different and shift away from $D_{12}/\omega = 1$. Generally, for $D_{12}/\omega = n$, the distribution of breakpoints is dependent on the parity of n , thus we term this phenomenon as odd-even effect. In Fig. 2 (e), we present T_{12} as a function of A under the conditions of $D_{12}/\omega = 1, 2$ and 3 for a better description of the odd-even effect. Here the transition amplitude display discrete peaks, with the intervals between peaks induced by ATS since the resonant transition is shifted due to the modulated effective coupling. For $D_{12}/\omega = 2$, the peaks are narrower compared to that of $D_{12}/\omega = 1$ and 3, indicating reduced overall absorption, and in agreement with the fact that the breakpoints are aligned to $D_{12}/\omega = 2$.

The origin of the odd-even effect is the longitudinal-driving-induced modulation of the effective coupling in H_{eff} . Assuming $g_1 J_{N-n} \ll g_2 J_N$, for the resonances of $D_{12} = n\omega$ and $D_{13} = n\omega$, the transitions are determined by r_- and r_+ , respectively. Assuming that Δ' is negli-

gible, we obtain r_- under the condition $D_{12} - n\omega = E_-$ and r_+ under the condition $D_{12} - n\omega = E_+$:

$$\begin{aligned} r_- &\propto \xi g_2 J_N - g_1 J_{N-n}(\Delta - E_-), \\ r_+ &\propto \xi g_2 J_N + g_1 J_{N-n}(E_+ - \Delta). \end{aligned} \quad (6)$$

By substituting in the expressions of Δ and ξ , and accounting for the condition $E_- = 0$, which means $D_{12} = n\omega$, we find $r_- \propto \sum_{m \neq N} g_1 g_2^2 (J_{m-n} J_m J_N - J_m^2 J_{N-n}) / (m\omega - D_{32})$ (see Appendix. D). In the large A/ω limit (i.e. strong driving), the asymptotic behavior of the Bessel functions dictates that for even n , $r_- \approx 0$. Thus transitions at $D_{12} = n\omega$ for large driving amplitude A is forbidden, yielding the so-called odd-even effect. This effect was experimentally observed in a DQD by Stehlik *et al.* [73], and explained based on an assumption of strong dissipation [36]. Our results here show that even without dissipation, the odd-even effect could also be observable because of the coherent destruction of tunneling in a multilevel system in the strong driving limit. We further discuss the odd-even effect with dissipation in Appendix E, which is in accordance with the result in Ref. 36 and 73.

IV. DARK STATE IN THE EFFECTIVE HAMILTONIAN

In atomic physics, dark state is the result of interference effects from transverse driving in a three-level Λ system [46]. When a system relaxes to the dark state, coherent population trapping would happen, which means the system will be trapped in the dark state and is decoupled from the excited state [46, 49–51, 53]. In our longitudinally driven system, off-diagonal coupling is also present in the effective Hamiltonian H_{eff} among the dressed states as a result of the higher-order LZS interference. Accordingly, when ξ is negligible, we expect

the dark state for our system to be

$$|\psi\rangle \propto g_2 J_N |1\rangle - g_1 J_{N-n} |2\rangle. \quad (7)$$

When the system is trapped in the dark state, the transition between $|\psi\rangle$ and $|3\rangle$ is strictly forbidden. Considering that state $|3\rangle$ has a different charge configuration from $|1\rangle$ and $|2\rangle$, forbidden transition to $|3\rangle$ means charge cannot transfer between the two dots, leading to a suppression in current through the DQD. In essence, coherent trapping here is caused by interference between the two paths of electron tunneling.

In Fig. 3 we demonstrate the emergence of the dark state by plotting the average transition amplitude $T_{\psi 3}$ from a random initial state $|\psi(\theta) = \cos(\theta)|1\rangle + \sin(\theta)|2\rangle$ to $|3\rangle$ with $g_{1,2} = 1$ GHz. In the vicinity of $D_{12} = 2\omega$ and $D_{13} = \omega$, the effective couplings are given by $\tilde{g}_{1,2} = g_{1,2} J_{\pm 1}(A/\omega)$, and the dark state $|\psi\rangle$ is then defined by $|\psi(\pi/4)\rangle$. Numerical simulation of averaged transition amplitude $T_{\psi 3}$ is shown in Fig. 3 (a), in which the suppression of transition amplitude is observed around $D_{12} = 2\omega$ for a wide range of A/ω . Two cross-sections with $A/\omega = 1.0$ and 8.0 are presented in Fig. 3 (b) and (c), respectively. These panels show that with increasingly strong driving A/ω , the contribution of the off-diagonal coupling ξ becomes less important, and $|\psi(\pi/4)\rangle$ becomes “darker”. For the state orthogonal to $|\psi(\pi/4)\rangle$, with $\tan(\theta) = -1$, a resonant peak appears as is shown in both Fig. 3 (b) and (c).

A similar three-level model can also be obtained from the five-level model based on the ST system. Thus we expect that similar features, including ATS, odd-even effect, and dark state, are all observable in the ST system as well.

V. QUANTUM GATES VIA THE DRIVING-INDUCED SYNTHETIC COUPLING

As shown in the effective Hamiltonian (3), the higher order interference among the three states produces a synthetic coupling ξ , which could be employed to generate quantum gates, and has the potential for fast operation. Here we demonstrate qubit control in a five-level ST system. Though the relevant H_{eff} is in principle for five states, nearby a resonance only three states are relevant as long as the difference between resonant frequencies is significantly greater than the synthetic couplings, so we will continue to use Eq. (3) as our starting point.

Different from the previous section, here we do need a precise driving amplitude, which restricts the leakage caused by $g_{1,2} J_\nu$ while ensures an accurate value of ξ . According to Eq. 3, leakage to the shuttle state is negligible as long as $|\delta| \gg |g_i J_\nu|$, while the spin manipulation time is determined by the strength of the synthetic coupling ξ . To suppress leakage, one can work in the large detuning regime [70, 71, 74], leading to a higher order of J_ν in H_{eff} . Unfortunately it also suppresses ξ , and is thus not a useful regime for quantum gates. On the other hand,

by tuning the driving amplitude A/ω , leakage can also be suppressed while maintaining a finite value for ξ . In other words, state manipulation can be implemented in the regime of small detuning, which adds the additional benefit of a greater exchange coupling strength in the ST system.

In Fig. 4(a) we present the transition amplitude between $|\uparrow, \uparrow\rangle \leftrightarrow |\uparrow, \downarrow\rangle$ (T_{12}) and $|\downarrow, \downarrow\rangle \leftrightarrow |\downarrow, \uparrow\rangle$ (T_{34}) versus frequency and detuning energy ε . At the solid triangle point with zero detuning, these two transitions are degenerate, which means that the spin rotations are independent of each other, and single-spin rotation can be generated. Otherwise, transitions occur at different driving frequencies, indicating that rotation of the spin on the right depends on the state of the left spin, which would lead to controlled rotation and two-spin gates.

In Fig. 4 (b) and (c), we calculate the time evolution operator $U(t)$ and present the time evolution of probability $P_{ij}(t) = |\langle i|U(t)|j\rangle|^2$. Fig. 4 (b) shows single-spin rotation with parameters $g_1 = 1$ GHz, $g_2 = 2$ GHz and amplitude of $A = 86.4$ GHz. The cross-section of the chevron at resonance exhibits high-fidelity exceeding 99.9% with fast manipulation time of 35 ns. When $\varepsilon \neq 0$, the two transitions shift differently as shown in Fig. 4 (a), and a controlled rotation can be generated. In Fig. 4(c), we present the controlled rotation with $\varepsilon \approx 26$ GHz as indicated by the red pentagram in Fig. 4(a) and $A = 20$ GHz. The result contains two overlapping chevrons — one is narrowly peaked at $\omega - D_{12} \approx -0.2$ GHz and one is broad peaked at $\omega - D_{12} \approx 0.2$ GHz. They are the consequence of T_{34} and T_{12} , respectively. The cross-section indicated by the black dashed line in Fig. 4 shows a resonant transition with amplitude over 99.5% and a suppressed off-resonant rotation amplitude of 0.4%. The frequency difference between the two resonant peaks indicates a significant exchange coupling, which is result of the small detuning.

VI. ADIABATIC STATE TRANSFER BY DRIVING AMPLITUDE MODULATION

In quantum optics, adiabatic state transfer is achieved via modulation of the coherent (transverse) couplings in a Λ model [48, 54, 55, 59]. It has been demonstrated in various systems [56–58], including in quantum dot spin chains in a mathematically isomorphic process called adiabatic quantum teleportation (AQT) [75, 76]. In our longitudinally driven system, to achieve state transfer we need to adiabatically modulate the effective Hamiltonian $H_{\text{eff}}(t)$, assuming that the modulation frequency is much smaller than the driving frequency. Compared to previous works where the off-diagonal coupling terms are tuned independently, g_i here are assumed to be constants in our model, leaving only the slow-varying amplitude $A(t)$ to be the control parameter.

In the following example, we accomplish adiabatic state transfer in a five-level ST system by amplitude mod-

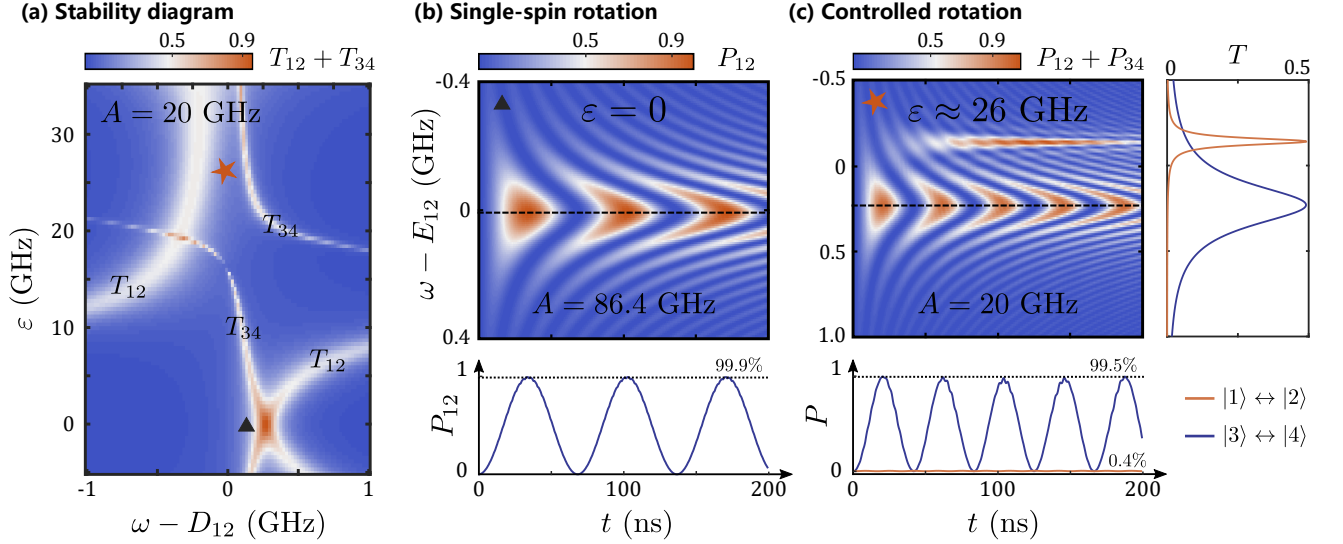


FIG. 4. **Quantum gate via Rabi oscillation in the ST system.** (a) Total transition amplitude $T_{12} + T_{34}$ versus detuning ε and driving frequency. Parameters used in simulation are $g_1 = 1$ GHz, $g_2 = 2$ GHz, $D_1 = -D_4 = 40$ GHz and $D_2 = -D_3 = 10$ GHz. (b) Rabi chevron for single-spin rotation with suppressed leakage with $\varepsilon = 0$, $A = 86.4$ GHz. The on-resonance oscillation at resonance exhibit of maximal amplitude over 99.9%. (c) The two-qubit conditional-rotation gate with $\varepsilon = 26$ GHz and $A = 20$ GHz, in which P_{12} and P_{34} resonant at different frequencies.

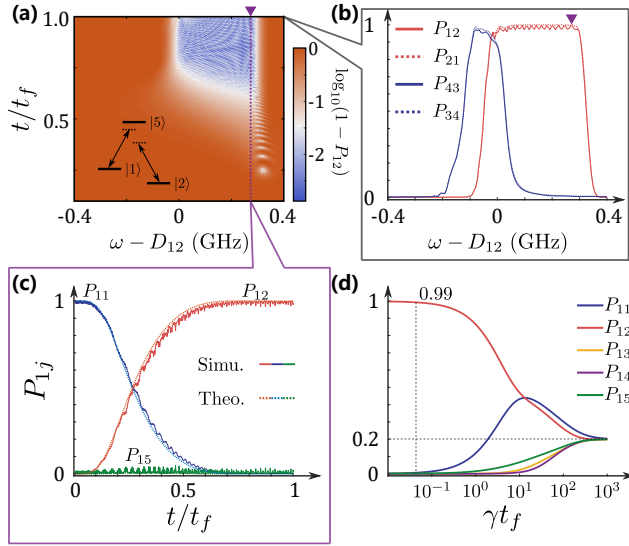


FIG. 5. **Quantum gate via an adiabatic passage in the ST system.** (a) Logarithm of infidelity $\log_{10}(1 - P_{12}(t))$ with respect to frequency derivation $\omega - D_{12}$. Inset shows the effective three-level model by $|1\rangle$, $|2\rangle$, and $|5\rangle$. (b) The final probability $P_{ij}(t_f)$ as a function of $\omega - D_{12}$, in which the triangle point can be used as the working point of controlled-rotation gate. (c) The cross-section along the dashed line in (a), from both full simulation of the time-dependent Hamiltonian (solid curves) and that by the effective Hamiltonian H_{eff} (dashed curves). (d) Probability with Lindblad dissipation strength γ . For $t_f < T_2/10$, transition amplitude $P_{12} > 99\%$; and for $t_f = T_2/20$ and in the long-time limit, state thermalization is reached, with $P_i = 1/5$ when $t_f > 10^2 T_2$.

ulation as

$$A(t) = 100 \sin^2(\pi t/2t_f), \quad 0 \leq t \leq t_f, \quad (8)$$

where $t_f = 1 \mu\text{s}$ is the total evolution time. This choice of $A(t)$ is for illustration purpose only and is not optimized. In the effective Hamiltonian, all the correlations such as ξ , Δ , and Δ' are included because when $A(t)$ is small, they may be important. We investigate the adiabatic process both through the effective Hamiltonian and by numerically solving the time-dependent Schrödinger equation with different driving frequencies. Similar to what we have discussed in the dark state section, here the effective model Hamiltonian is equivalent to that for a three-level Λ configuration composed of $|1\rangle$, $|2\rangle$ and $|5\rangle$, while the effective couplings are only tuned by driving amplitude via the Bessel functions.

With a modulation on the driving amplitude, state transfer occurs in a wide range of driving frequencies as shown in Fig. 5 (a), where the color code represents the logarithm of infidelity $1 - P_{12}(t)$. In Fig. 5 (b) we present different probabilities $P_{ij}(t_f)$ with the same adiabatic passage as a function of driving frequency. Based on the fact that transitions are addressable via driving frequency, controlled rotation can be constructed. For example, when $\omega - D_{12} = 0.27$ GHz as is labeled by the solid purple triangle in both Fig. 5 (a) and (b), P_{12} and P_{21} are significant while P_{34} P_{43} are minimal. In addition, the plateau of $P_{ij}(t_f)$ indicates that the adiabatic state transfer is robust to frequency/energy spacing shift. In Fig. 5 (c), we compare the time evolution from our full numerical simulation with the results from $H_{\text{eff}}(t)$ for a given driving frequency ω , along the dashed vertical line in Fig. 5 (a). We find good agreements between the

two approaches. In Appendix C, we show that H_{eff} in Eq. 3 is a more robust and faithful representation of the original time-dependent Hamiltonian than that from the high-frequency expansion [38].

In a semiconductor QD system, dephasing is usually quite fast, especially among states with different charge distributions. We thus also investigated its influence on our adiabatic state transfer protocol, described by the following Lindblad master equation

$$\dot{\rho} = -i[H(t), \rho] + \sum_{k \neq 0} \left[L_k \rho L_k^\dagger - \frac{1}{2} \{L_k^\dagger L_k, \rho\} \right], \quad (9)$$

where the summation represents the non-unitary evolution and $L_k = \sqrt{\nu_k} |k\rangle\langle k|$, for $k = 1, \dots, 5$, account for the white-noise fluctuations on each level. We neglect the contribution of energy relaxation between these levels for the reason that in QDs, $T_1 \gg T_2$. In Fig. 5 (d) we plot $P_{1j}(t_f)$ as a function of γ (assuming $\nu_k = \gamma = 1/T_2$), showing a transition from the perfect state transfer with $P_{12}(t_f) \rightarrow 1$ to $P_{1j} = 1/5$ as the maximal mixed state, which can be reached when $t_f > 10^2 T_2$. If the protocol time is much shorter than dephasing time, for example when $t_f = T_2/20$, the fidelity $P_{12}(t_f)$ can exceed 0.99, as expected.

VII. CONCLUSION

In conclusion, we have introduced Floquet engineering to gate-defined DQDs system. In particular, we develop a universal approach that allows us to study the evolution of a multilevel system under strong longitudinal drive. We show that the resulting multilevel LZS interference is well described by an effective three-level model, and is fully-tunable by the driving field. Employing this effective model, we demonstrate phenomena that are qualitatively similar to ATS and dark state, but have distinct features because they are the results of longitudinal instead of transverse driving. We are able to understand the so-called odd-even effect caused by coherent destruction of tunneling within our effective model. We also demonstrate fast quantum gates based on the interference-induced synthetic coupling in a five-level ST system, and show that qubit manipulation with a broadband driving can be realized by adiabatic passage.

Our results clearly demonstrate that coherent longitudinal driving and the resulting LZS interference in a multilevel quantum system can lead to strong tunability, since coherent phases in the LZS process are controlled by the driving field. In the context of quantum dot devices, such tunability should be readily available for hybrid qubits and singlet-triplet qubits, and can be employed in any multi-dot device where tunnel couplings cannot be tuned conveniently. Though we focus on a sinusoidal driving field in this initial study, our approach can be extended to any periodic driving field after a Fourier expansion. Most importantly, the theoretical considerations

we present here is quite general and should be valid for a variety of multilevel systems that are experimentally relevant.

VIII. ACKNOWLEDGMENTS

This work was supported by the National Natural Science Foundation of China (Grants No. 12074368, 92165207, 12034018 and 61922074), the Anhui Province Natural Science Foundation (Grants No. 2108085J03), and the USTC Tang Scholarship. X.H. acknowledges financial support by U.S. ARO through grant W911NF1710257.

Appendix A: Derivation of effective Hamiltonian

1. Rotating frame for diagonal modulated system

We are dealing with a time-periodic system with strong diagonal modulation ($A \gg \omega$), which cannot be treated conveniently using Floquet theorem in our searching of a time-independent H_{eff} . To make this system more conveniently treatable by Floquet theorem, we first perform a proper rotation of H by

$$U = \text{diag}(e^{i(D_2+n\omega)t}, e^{iD_2t}, e^{i(D_2+N\omega)t - i\frac{A \sin(t\omega)}{\omega}}). \quad (\text{A1})$$

The resulting Hamiltonian takes the form

$$\tilde{H}(t) = \begin{pmatrix} D_{12} - n\omega & & c(t)g_1 e^{in\omega t} \\ & 0 & c(t)g_2 \\ c^*(t)g_1 e^{-in\omega t} & c^*(t)g_2 & D_{32} - N\omega \end{pmatrix}, \quad (\text{A2})$$

with $c(t) = e^{i\frac{A \sin(\omega t)}{\omega} - iN\omega t} = \sum_{\nu} J_{\nu}(A/\omega) e^{i(\nu-N)\omega t}$. By ‘‘proper’’, we mean that (i) the diagonal matrix elements should be restricted to the first Brillouin zone; (ii) the new Hamiltonian $\tilde{H}(t)$ should have the same periodicity as $H(t)$, and (iii) the degrees of freedom in U should be uniquely determined. The time dependence of $\tilde{H}(t)$ is now more conveniently located in the off-diagonal terms.

2. Floquet-Schrödinger equation and numerical simulation

The Floquet theorem provides a general framework to study the linear models with periodic modulation in the time domain [65], and it has also been exploited to study dissipative systems [77]. In this work, some simulation is carried out based on the non-dissipative Floquet theorem, as we would present in this subsection. For $i\partial_t |\psi\rangle = \tilde{H}(t) |\psi\rangle$, where $\tilde{H}(t)$ was defined above, we can write $|\psi\rangle = e^{-iqt} |u(t)\rangle$, where q is the quasi-energy and $|u(t)\rangle$ is a periodic function with period T . We now have

$$(\tilde{H}(t) - i\partial_t) |u(t)\rangle = q |u(t)\rangle, \quad |u(t)\rangle = |u(t+T)\rangle. \quad (\text{A3})$$

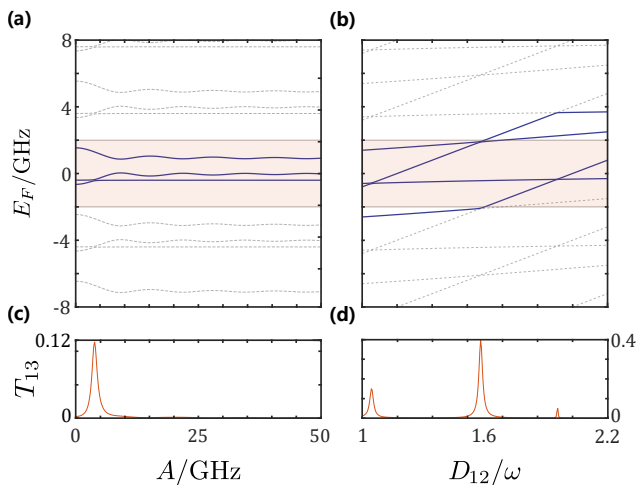


FIG. 6. Floquet energy levels E_F and transition amplitude T_{13} versus A in (a) and D_{12} in (b), respectively. The energy levels are presented in solid blue or dashed gray lines, while the red shading area indicates the first Brillouin zone. The energy structure shows a periodicity as Floquet theorem indicated. When energy levels crossover with each other, state transfer occurs, thus population in $|\beta\rangle$ can be detected as indicated by solid red lines in (c) and (d).

This equation can be cast into a stationary equation, assuming that $|u(t)\rangle = \sum_{\alpha,n} c_{n\alpha} |\alpha, n\rangle$, where $|\alpha, n\rangle = e^{in\omega t} |\alpha\rangle$. If one takes (\mathcal{U}) as a column matrix consisting of all the $c_{n\alpha}$ in proper order with $n \in \mathbb{Z}$, we find the Floquet-Schrödinger equation in the matrix form as $\mathcal{H}_F(\mathcal{U}) = q(\mathcal{U})$, with matrix elements

$$\langle \alpha, n | \mathcal{H}_F | \beta, m \rangle = \tilde{H}_{\alpha\beta}^{(n-m)} + n\omega \delta_{nm} \delta_{\alpha\beta}, \quad (\text{A4})$$

where $\tilde{H}_{\alpha\beta}^{(n-m)}$ is the $(n-m)$ th Fourier coefficient of matrix element $\tilde{H}_{\alpha\beta}$. Though \mathcal{H}_F is a matrix of infinite size, in numerical simulations we can make a truncation for n (in our case we choose $|n| \leq N_c = 20$) to calculate the quasienergy q , which is shown in Fig. 6 (a)-(b). As expected, the spectrum is a repeating of levels in the first Brillouin zone shifted by ω . We will in general focus on the first Brillouin zone defined as $\mathcal{B} = [-\omega/2, \omega/2]$.

Based on \mathcal{H}_F , we can evaluate the transition amplitude from $|\beta\rangle$ to $|\alpha\rangle$ by

$$U_{\alpha,\beta}(t; t_0) = \sum_n \langle \alpha, n | e^{-i\mathcal{H}_F(t-t_0)} | \beta, 0 \rangle e^{in\omega t}, \quad (\text{A5})$$

where the summation collects contributions from all orders of Fourier components. The averaged transition amplitude is then given by

$$\begin{aligned} T_{\alpha\beta}(t_0) &= \lim_{t \rightarrow \infty} \frac{1}{t} \int_0^t |U_{\alpha,\beta}(\tau; t_0)|^2 d\tau \\ &= \sum_{m,n,\phi} \langle \alpha, n | \phi \rangle \langle \phi | \beta, 0 \rangle \langle \beta, m | \phi \rangle \langle \phi | \alpha, n \rangle e^{im\omega t_0}, \end{aligned} \quad (\text{A6})$$

$$(\text{A7})$$

with $|\phi\rangle$ the eigenstates of \mathcal{H}_F . Our numerical results for this transition amplitude are shown in Fig. 6 (c) and (d), where resonance transitions are expected at degeneracy points.

Appendix B: Effective Hamiltonian

We mainly present our results based on an effective Hamiltonian H_{eff} by eliminating the off-diagonal couplings between different Brillouin zones in \mathcal{H}_F to the lowest order. This is achieved by Löwdin's quasi-degenerate perturbation theory via a unitary transformation of $\tilde{\mathcal{H}}_F = U^\dagger \mathcal{H}_F U$, where $U = e^{-S}$, and S is given by [66]

$$S_{ml} = \frac{(\mathcal{H}_F)_{ml}}{(\mathcal{H}_F)_{ll} - (\mathcal{H}_F)_{mm}}. \quad (\text{B1})$$

Here m and l include indices n and α in Eq. A4.

The effective Hamiltonian H_{eff} in the main text is thus obtained, in which Δ' , Δ , ξ are corrections induced by the couplings to the higher Brillouin zones:

$$\Delta' = \sum_{m \neq N-n} \frac{(g_1 J_m)^2}{D_{13} + m\omega}, \quad \Delta = \sum_{m \neq N} \frac{(g_2 J_m)^2}{D_{23} + m\omega} \quad (\text{B2})$$

$$\xi = \sum_{m \neq N} \frac{g_1 g_2 J_m J_{m-n}}{2(D_{23} + m\omega)} + \sum_{m \neq N-n} \frac{g_1 g_2 J_m J_{m+n}}{2(D_{13} + m\omega)}. \quad (\text{B3})$$

Appendix C: Comparison of different theoretical approaches

In Ref. 38, a universal effective model for a driven system was obtained based on high-frequency expansion. Here we compare our effective model with this established model, and clarify how they are consistent with or different from each other.

The objective in deriving an effective model is to find a basis in which the originally time-dependent Hamiltonian becomes approximately time-independent, so that the associated eigenstates are stationary. This approach is exemplarily shown in going to the rotating frame when treating conventional nuclear magnetic resonance. Here we show that the basis found in our approach is closer to reaching this objective, such that dynamics based on our effective Hamiltonian is more consistent with numerical simulations under wider range of conditions.

According to the reference, one can find a rotation $e^{-iK(t)}$ such that $H_r = e^{-iK(t)} H(t) e^{iK(t)}$ is time-independent. Following the same rotation defined by U above, one can write $H(t) = H_0 + \sum_{n \neq 0} H_n e^{in\omega t}$, and, the effective Hamiltonian H_r is obtained as

$$H_r = H_0 + \frac{1}{2} \sum_{n \neq 0} \frac{[H_n, H_{-n}]}{n\omega} + \dots \quad (\text{C1})$$

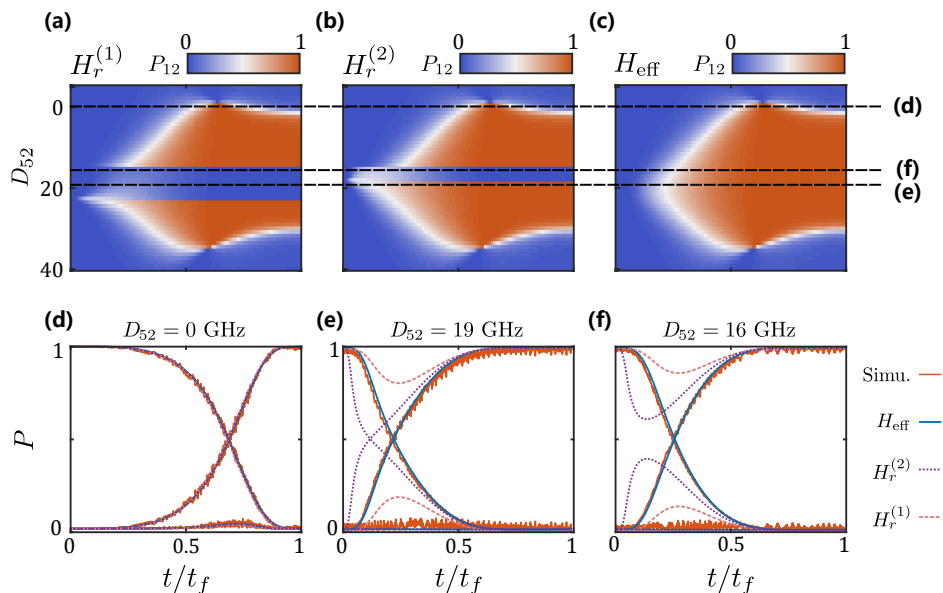


FIG. 7. **Comparison of two effective Hamiltonians.** Adiabatic state transfer is investigated to clarify the difference between two models. We simulate the ideal adiabatic state transfer as a function of detuning D_{52} based on three different models – first-order $H_r^{(1)}$ (a), second-order $H_r^{(2)}$ (b), and our effective model H_{eff} (c). For clarity, we present three cross-sections labeled by dashed lines in (d), (e), and (f). H_{eff} faithfully represents the dynamics in (d), (e) and (f), while $H_r^{(1,2)}$ only accurate in (d).

The H_r thus obtained is equivalent to our H_{eff} when D_{12} and D_{52} are integer multiples of ω , but is otherwise different. To demonstrate their differences quantitatively, we repeat the numerical simulations as presented in Fig. 5 (c). Here we keep $D_{12} \approx \omega$, while varying D_{52} , and compare results given by the two models and the original time-dependent Hamiltonian. For clarity, we denote the results derived by Ref. 38 as $H_r^{(1)}$ and $H_r^{(2)}$ for first- and second-order approximation, respectively.

In Fig. 7 (a), (b), and (c) we track the transfer probability P_{12} as a function of D_{52} and evolution time t . A gap appears in both (a) and (b), meaning that no transfer occurs when D_{52} is in that range, while there is no gap in the results obtained from H_{eff} in (c). Furthermore, the gap in the results given by $H_r^{(2)}$ is narrower than that given by $H_r^{(1)}$. In Fig. 7 (d), (e), and (f) we choose three cross-sections denoted by dashed lines in (a), (b), and (c) to demonstrate how the different models differ. For $D_{52} = 0$, presented in panel (d), $H_r^{(1)}$ is equivalent to H_{eff} , while $H_r^{(2)}$ gives no correction to $H_r^{(1)}$. All three models are consistent with the direct numerical simulation. However, when $D_{52} \neq 0$, difference arises between $H_r^{(1,2)}$ and H_{eff} . In Fig. 7 (e), only H_{eff} is quantitatively consistent with the numerical simulation, while $H_r^{(2)}$ is only qualitatively consistent. The results from $H_r^{(1)}$, on the other hand, are qualitatively different from the simulation results, with no population transfer at the long time limit. When $D_{52} = 16$ GHz, as presented in Fig. 7 (f), both $H_r^{(1,2)}$ now fail to capture the adiabatic state

transfer process, while H_{eff} still works well and track the numerical simulation perfectly.

To further accentuate the differences between the two effective Hamiltonians, below we derive our H_{eff} using a procedure similar to that in Ref. 38. Different from Ref. 38, here we prove that for any e^{iqt} (q being an operator, thus a matrix when the basis states are chosen), there exists an operator $K(t)$ and a rotation $e^{-iK(t)}$, such that $e^{iK(t)}e^{iqt}H(t)e^{-iqt}e^{-iK(t)} \approx e^{iqt}H_{\text{eff}}e^{-iqt}$, where H_{eff} is time-independent. For convenience, we denote

$$H'(t) = e^{iqt}H(t)e^{-iqt} \quad (\text{C2})$$

$$= e^{iqt} \left(H_0 + \sum_{n \neq 0} H_n e^{in\omega t} \right) e^{-iqt} \quad (\text{C3})$$

$$= H'_0 + \sum_{n \neq 0} H'_n e^{in\omega t}. \quad (\text{C4})$$

Unlike the periodic $H(t)$, $H'(t)$ here is quasi periodic. The objective now is to find a $K(t)$ such that $e^{iK(t)}H'(t)e^{-iK(t)}$ is independent of ω rather than t . In this way, we find that

$$\partial_t K \approx \sum_{n \neq 0} H'_n e^{in\omega t}. \quad (\text{C5})$$

If we further suppose q is diagonal as $q = \text{diag}\{q_1, \dots, q_n\}$, we obtain

$$H_{\text{eff}} \approx H_0 + \frac{1}{2} \sum_{n \neq 0} [Q_n, H_{-n}], \quad (\text{C6})$$

where

$$Q_n = \sum_{j,j'} \frac{(H_n)_{jj'}}{n\omega + q_j - q_{j'}} |j\rangle\langle j'|. \quad (\text{C7})$$

When q_i are set as D_i , one obtains H_{eff} presented in the main text. On the other hand, if q is set as the identity matrix, one obtains H_r . Both H_{eff} and H_r is time-independent. However, from the perspective of perturbation theory, H_r does not take the energy difference $D_i - D_j$ into consideration, and is thus not as accurate as H_{eff} whenever these energy differences are significant. For example, when $n\omega \gg |D_i - D_j|$, H_r is approximately equivalent to H_{eff} . In contrast, when $|D_i - D_j|$ is comparable to $n\omega$, H_r is no longer accurate.

In short, the analytical analysis presented here and comparisons with numerical simulations show that our effective model H_{eff} is a faithful representation of the dynamics of the longitudinally driven multi-level system. On the other hand, while the high-frequency expansion is an elegant theoretical approach, the resulting effective Hamiltonian often fails to catch the important features of the original driven system.

Appendix D: ATS and odd-even effect

To address the resonant transition presented in the main text, we diagonalize the subspace of $\{|2\rangle, |3\rangle\}$ into $\{|+\rangle, |-\rangle\}$. Effective Hamiltonian is then given by

$$H_{\text{eff}} = \begin{pmatrix} D_{12} - n\omega & r_+ & r_- \\ r_+^* & E_+ & 0 \\ r_-^* & 0 & E_- \end{pmatrix}, \quad (\text{D1})$$

with E_{\pm} the eigenenergies of subspace spanned by $\{|2\rangle, |3\rangle\}$ and r_{\pm} the corresponding coupling strength. For weak couplings, the resonant condition is determined by $D_{12} - n\omega = E_{\pm}$, resulting in the ATS induced by longitudinal drive as mentioned in the main text. Notice that the resonant condition indicates state manipulation based on multifrequency. To demonstrate that, we present a numerical simulation result in Fig. 8 (a), (b), where we present Rabi oscillation for $D_{12} = \omega$ and $D_{12} = 2\omega$.

Analogue to coherent destruction of tunneling in TLS, intervals are found when the relevant effective coupling term meets its zero points, and interestingly, the Bessel functions induce a parity-dependent result, which is referred to as odd-even effect in the main text. According to H_{eff} , the resonance is described by $D_{12} - n\omega = E_{\pm}$. One of the branches, namely, $D_{12} - n\omega \approx 0$, reflects the parity effect. e.g., for $D_{12} = n\omega$, we have

$$\begin{aligned} r_- &\propto \xi g_2 J_N - g_1 J_{N-n} \Delta \\ &= \sum_{m \neq N} \frac{g_1 g_2^2}{m\omega - D_{23}} (J_{m-n} J_m J_N - J_m^2 J_{N-n}), \end{aligned} \quad (\text{D2})$$

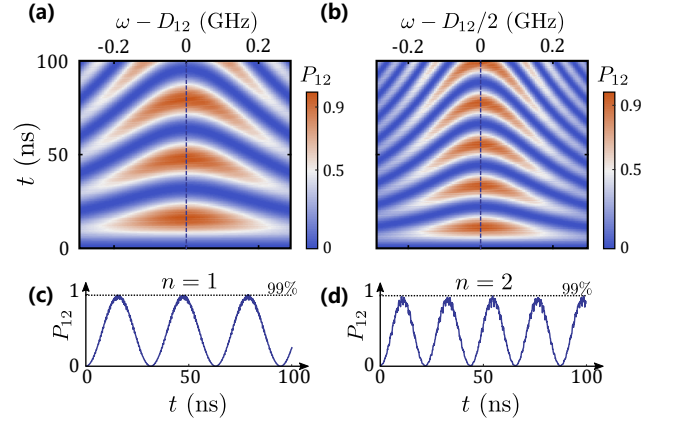


FIG. 8. **Rabi oscillation based on higher harmonic resonance.** Rabi oscillation chevrons for $n = 1$ (a) and $n = 2$ (b), resonant oscillation amplitude of which is presented in (c) and (d) respectively.

on the other hand, for the other branch, in the vicinity of $D_{13} = (N - n)\omega$, we have

$$\begin{aligned} r_+ &\propto \sum_{m \neq N} \frac{g_1 g_2^2 J_m J_{m-n} J_N}{2(D_{23} + m\omega)} + \sum_{m \neq N-n} \frac{g_1 g_2^2 J_m J_{m+n} J_N}{2(m + n - N)\omega} \\ &+ g_1 J_N \left(D_{32} - N\omega - \sum_{m \neq N} \frac{(g_2 J_m)^2}{D_{23} + N\omega} \right) \end{aligned} \quad (\text{D3})$$

For Bessel functions of the first kind, we know the asymptotic behavior of

$$J_n(x) \approx \sqrt{\frac{2}{\pi x}} \cos[x - (2n + 1)\pi/4], \quad x \gg n. \quad (\text{D4})$$

This guarantees $r_- \approx 0$ at $D_{12} = n\omega$ for even ns when $A/\omega \gg N - n$, $m - n$, while for odd ns , break points can be found around $D_{12} = n\omega$ when $J_{m-n} J_N = J_m J_{N-n}$, but this condition could not always be fulfilled. However, odd-even effect would disappear when $\varepsilon > A$, i.e., when system does not go through anti-crossings, which is in accordance with experiment [73]. It can be interpreted with the relation $N \approx D_{23}/\omega > A/\omega$, which means $\varepsilon > A$ undermines the approximation condition $A/\omega \gg N - n$ for small n .

Appendix E: Odd-even effect with dissipation in strong driving limit

In this section, we would demonstrate how the ATS in the main text eventually yields the odd-even effect reported by Ref. 73 by introducing dissipation and strong driving. Based on the fact that shuttle state $|3\rangle$ can be detected electrically, we calculate $P_{13}(t)$ by Lindblad master equation with and without dissipation under different driving amplitude, and average $P_{13}(t)$ over 800 ns to obtain T_{13} approximately. The dissipation is involved

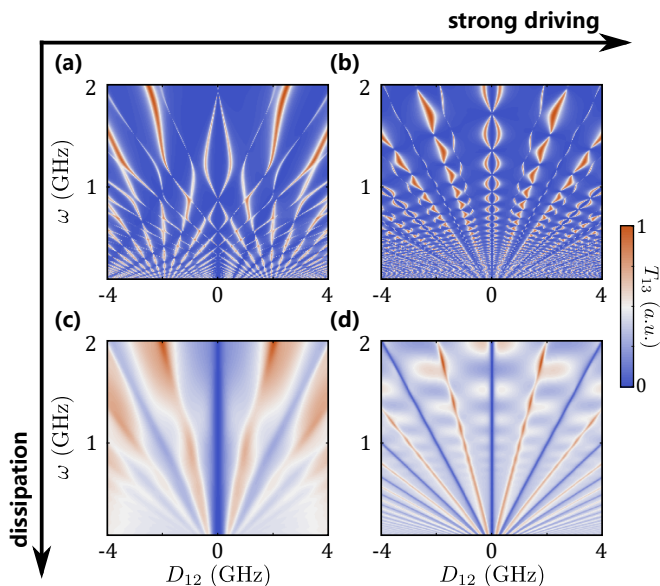


FIG. 9. **ATS signal versus D_{12} and ω in different situations.** We compare ATS without dissipation under different driving amplitude, i.e., 4 GHz in (a) and 20 GHz in (b). We also repeat this comparison with dissipation, and the relevant results are presented in (c) and (d).

by considering a dephasing on each state at a rate of

$\gamma = 0.01$ GHz and electron jump in and out of DQDs at a rate of $\Gamma = 1$ GHz. We calculate T_{13} as a function of driving frequency ω and energy difference D_{12} , and the result is presented in Fig. 9.

We present the ATS signal under a driving amplitude of 4 GHz and 20 GHz in Fig. 9 (a) and (b), respectively. With the increasing of the driving amplitude, the splitting of ATS signal saturates. As one could expect, when the driving field is sufficiently strong, resonant transition only happens at $D_{12} = n\omega$ or $D_{13} = m\omega$. Furthermore, as discussed in the main text, for $D_{12} = 2n\omega$, transition from $|1\rangle$ to $|-\rangle$ is almost forbidden (determined by r_-). In this context, even orders of harmonics are supposed to vanish in strong driving limit, which yields the so-called odd-even effect. Hence, we take dissipation into consideration and repeat the simulation. The results are presented in Fig. 9 (c), (d), corresponding to (a) and (b), respectively. The dissipation yields a background signal and broadens the resonant transition signal. On the basis of the background signal, we see harmonics of different orders, and the odd-even effect is obvious. i.e., even orders manifests as a dip meanwhile for odd orders, there is a peak. The results presented in Fig. 9 (d) almost reproduces the phenomenon in Ref. 73 and the theoretical result in Ref. 36. Comparing to the former works, we present a more insightful interpretation for such odd-even effect by effective Hamiltonian.

-
- [1] F. Arute, K. Arya, R. Babbush, D. Bacon, J. C. Bardin, *et al.*, Quantum supremacy using a programmable superconducting processor, *Nature* **574**, 505 (2019).
 - [2] C. Figgatt, A. Ostrander, N. M. Linke, K. A. Landsman, D. Zhu, D. Maslov, and C. Monroe, Parallel entangling operations on a universal ion-trap quantum computer, *Nature* **572**, 368 (2019).
 - [3] F. Arute, K. Arya, R. Babbush, D. Bacon, J. C. Bardin, *et al.*, Hartree-fock on a superconducting qubit quantum computer, *Science* **369**, 1084 (2020).
 - [4] L. Egan, D. M. Debroy, C. Noel, A. Risinger, D. Zhu, D. Biswas, M. Newman, M. Li, K. R. Brown, M. Cetina, and C. Monroe, Fault-tolerant control of an error-corrected qubit, *Nature* **598**, 281 (2021).
 - [5] Y. Wu, W.-S. Bao, S. Cao, F. Chen, M.-C. Chen, *et al.*, Strong Quantum Computational Advantage Using a Superconducting Quantum Processor, *Phys. Rev. Lett.* **127**, 180501 (2021).
 - [6] N. W. Hendrickx, W. I. Lawrie, M. Russ, F. van Riggelen, S. L. de Snoo, R. N. Schouten, A. Sammak, G. Scappucci, and M. Veldhorst, A four-qubit germanium quantum processor, *Nature* **591**, 580 (2021).
 - [7] A. R. Mills, C. R. Guinn, M. J. Gullans, A. J. Sigillito, M. M. Feldman, E. Nielsen, and J. R. Petta, Two-qubit silicon quantum processor with operation fidelity exceeding 99%, *Science Advances* **8**, eabn5130 (2022).
 - [8] A. Noiri, K. Takeda, T. Nakajima, T. Kobayashi, A. Sammak, G. Scappucci, and S. Tarucha, Fast universal quantum gate above the fault-tolerance threshold in silicon, *Nature* **601**, 338 (2022).
 - [9] X. Xue, M. Russ, N. Samkharadze, B. Undseth, A. Sammak, G. Scappucci, and L. M. K. Vandersypen, Quantum logic with spin qubits crossing the surface code threshold, *Nature* **601**, 343 (2022).
 - [10] M. T. Mądzik, S. Asaad, A. Youssef, B. Joecker, K. M. Rudinger, E. Nielsen, K. C. Young, T. J. Proctor, A. D. Baczewski, A. Laucht, V. Schmitt, F. E. Hudson, K. M. Itoh, A. M. Jakob, B. C. Johnson, D. N. Jamieson, A. S. Dzurak, C. Ferrie, R. Blume-Kohout, and A. Morello, Precision tomography of a three-qubit donor quantum processor in silicon, *Nature* **601**, 348 (2022).
 - [11] M. Bukov, L. D'Alessio, and A. Polkovnikov, Universal high-frequency behavior of periodically driven systems: from dynamical stabilization to Floquet engineering, *Adv. Phys.* **64**, 139 (2015).
 - [12] T. Oka and S. Kitamura, Floquet engineering of quantum materials, *Annual Review of Condensed Matter Physics* **10**, 387 (2019).
 - [13] M. S. Rudner and N. H. Lindner, Band structure engineering and non-equilibrium dynamics in Floquet topological insulators, *Nat. Rev. Phys.* **2**, 229 (2020).
 - [14] C. Weitenberg and J. Simonet, Tailoring quantum gases by Floquet engineering, *Nat. Phys.* **17**, 1342 (2021).
 - [15] K. Jiménez-García, L. J. Leblanc, R. A. Williams, M. C. Beeler, C. Qu, M. Gong, C. Zhang, and I. B. Spielman, Tunable spin-orbit coupling via strong driving in ultracold-atom systems, *Phys. Rev. Lett.* **114**, 1 (2015).
 - [16] L. W. Clark, N. Jia, N. Schine, C. Baum, A. Georgakopoulos, and J. Simon, Interacting Floquet polaritons, *Nature* **571**, 532 (2019).

- [17] D.-W. Wang, C. Song, W. Feng, H. Cai, D. Xu, H. Deng, H. Li, D. Zheng, X. Zhu, H. Wang, S.-Y. Y. Zhu, and M. O. Scully, Synthesis of antisymmetric spin exchange interaction and chiral spin clusters in superconducting circuits, *Nat. Phys.* **15**, 382 (2019).
- [18] A. Laucht, R. Kalra, S. Simmons, J. P. Dehollain, J. T. Muhonen, F. A. Mohiyaddin, S. Freer, F. E. Hudson, K. M. Itoh, D. N. Jamieson, J. C. McCallum, A. S. Dzurak, and A. Morello, A dressed spin qubit in silicon, *Nat. Nanotechnol.* **12**, 61 (2017).
- [19] J. M. Nichol, L. A. Orona, S. P. Harvey, S. Fallahi, G. C. Gardner, M. J. Manfra, and A. Yacoby, High-fidelity entangling gate for double-quantum-dot spin qubits, *npj Quantum Inf.* **3**, 3 (2017).
- [20] P. Huang and X. Hu, Electric-dipole-induced resonance and decoherence of a dressed spin in a quantum dot (2021), [arXiv:2103.05817](https://arxiv.org/abs/2103.05817) [[cond-mat.mes-hall](https://arxiv.org/archive/cond)].
- [21] M. A. Nakonechnyi, D. S. Karpov, A. N. Omelyanchouk, and S. N. Shevchenko, Multi-signal spectroscopy of qubit-resonator systems, *Low Temperature Physics* **47**, 383 (2021).
- [22] S. Shevchenko, S. Ashhab, and F. Nori, Landau-Zener-Stückelberg interferometry, *Phys. Rep.* **492**, 1 (2010).
- [23] M. P. Silveri, J. A. Tuorila, E. V. Thuneberg, and G. S. Paraoanu, Quantum systems under frequency modulation, *Reports Prog. Phys.* **80**, 056002 (2017).
- [24] O. V. Ivakhnenko, S. N. Shevchenko, and F. Nori, Quantum Control via Landau-Zener-Stückelberg-Majorana Transitions (2022), [arXiv:2203.16348](https://arxiv.org/abs/2203.16348) [[cond-mat.mes-hall](https://arxiv.org/archive/cond)].
- [25] W. D. Oliver, Mach-Zehnder Interferometry in a Strongly Driven Superconducting Qubit, *Science* **310**, 1653 (2005).
- [26] D. M. Berns, M. S. Rudner, S. O. Valenzuela, K. K. Berggren, W. D. Oliver, L. S. Levitov, and T. P. Orlando, Amplitude spectroscopy of a solid-state artificial atom, *Nature* **455**, 51 (2008).
- [27] W. D. Oliver and S. O. Valenzuela, Large-amplitude driving of a superconducting artificial atom, *Quantum Inf. Process.* **8**, 261 (2009).
- [28] G. Cao, H.-O. Li, T. Tu, L. Wang, C. Zhou, M. Xiao, G.-C. Guo, H.-W. Jiang, and G.-P. Guo, Ultrafast universal quantum control of a quantum-dot charge qubit using Landau-Zener-Stückelberg interference, *Nat. Commun.* **4**, 1401 (2013).
- [29] J. Stehlik, Y. Dovzhenko, J. R. Petta, J. R. Johansson, F. Nori, H. Lu, and A. C. Gossard, Landau-Zener-Stückelberg interferometry of a single electron charge qubit, *Phys. Rev. B* **86**, 121303 (2012).
- [30] F. Forster, G. Petersen, S. Manus, P. Hänggi, D. Schuh, W. Wegscheider, S. Kohler, and S. Ludwig, Characterization of qubit dephasing by Landau-Zener-Stückelberg-Majorana interferometry, *Phys. Rev. Lett.* **112**, 116803 (2014).
- [31] P. Huang, J. Zhou, F. Fang, X. Kong, X. Xu, C. Ju, and J. Du, Landau-Zener-Stückelberg interferometry of a single electron spin in a noisy environment, *Phys. Rev. X* **1**, 1 (2011).
- [32] X. Mi, S. Kohler, and J. R. Petta, Landau-Zener interferometry of valley-orbit states in Si/SiGe double quantum dots, *Phys. Rev. B* **98**, 161404 (2018).
- [33] S. N. Shevchenko, A. I. Ryzhov, and F. Nori, Low-frequency spectroscopy for quantum multilevel systems, *Phys. Rev. B* **98**, 195434 (2018).
- [34] A. Bogan, S. Studenikin, M. Korkusinski, L. Gaudreau, P. Zawadzki, A. S. Sachrajda, L. Tracy, J. Reno, and T. Hargett, Landau-Zener-Stückelberg-Majorana Interferometry of a Single Hole, *Phys. Rev. Lett.* **120**, 207701 (2018).
- [35] G. Sun, X. Wen, B. Mao, J. Chen, Y. Yu, P. Wu, and S. Han, Tunable quantum beam splitters for coherent manipulation of a solid-state tripartite qubit system, *Nat. Commun.* **1**, 51 (2010).
- [36] J. Danon and M. S. Rudner, Multilevel interference resonances in strongly driven three-level systems, *Phys. Rev. Lett.* **113**, 247002 (2014).
- [37] S. Rahav, I. Gilary, and S. Fishman, Effective Hamiltonians for periodically driven systems, *Phys. Rev. A* **68**, 013820 (2003).
- [38] N. Goldman and J. Dalibard, Periodically Driven Quantum Systems: Effective Hamiltonians and Engineered Gauge Fields, *Phys. Rev. X* **4**, 031027 (2014).
- [39] A. Eckardt and E. Anisimovas, High-frequency approximation for periodically driven quantum systems from a Floquet-space perspective, *New J. Phys.* **17**, 093039 (2015).
- [40] X. Zhang, H.-O. Li, G. Cao, M. Xiao, G.-C. Guo, and G.-P. Guo, Semiconductor quantum computation, *Nat. Sci. Rev.* **6**, 32 (2019).
- [41] L. Petit, H. G. J. Eenink, M. Russ, W. I. L. Lawrie, N. W. Hendrickx, S. G. J. Philips, J. S. Clarke, L. M. K. Vandersypen, and M. Veldhorst, Universal quantum logic in hot silicon qubits, *Nature* **580**, 355 (2020).
- [42] C. H. Yang, R. C. C. Leon, J. C. C. Hwang, A. Saraiva, T. Tanttu, W. Huang, J. Camirand Lemyre, K. W. Chan, K. Y. Tan, F. E. Hudson, K. M. Itoh, A. Morello, M. Pioro-Ladrière, A. Laucht, and A. S. Dzurak, Operation of a silicon quantum processor unit cell above one kelvin, *Nature* **580**, 350 (2020).
- [43] S. H. Autler and C. H. Townes, Stark effect in rapidly varying fields, *Phys. Rev.* **100**, 703 (1955).
- [44] X. Xu, B. Sun, P. R. Berman, D. G. Steel, A. S. Bracker, D. Gammon, and L. J. Sham, Coherent Optical Spectroscopy of a Strongly Driven Quantum Dot, *Science* **317**, 929 (2007).
- [45] M. A. Sillanpää, J. Li, K. Cicak, F. Altomare, J. I. Park, R. W. Simmonds, G. S. Paraoanu, and P. J. Hakonen, Autler-Townes Effect in a Superconducting Three-Level System, *Phys. Rev. Lett.* **103**, 193601 (2009).
- [46] H. R. Gray, R. M. Whitley, and C. R. Stroud, Coherent trapping of atomic populations, *Opt. Lett.* **3**, 218 (1978).
- [47] K.-J. Boller, A. Imamoglu, and S. E. Harris, Observation of electromagnetically induced transparency, *Phys. Rev. Lett.* **66**, 2593 (1991).
- [48] M. O. Scully and M. S. Zubairy, *Quantum Optics* (Cambridge University Press, 1997).
- [49] C. Wei and N. B. Manson, Observation of the dynamic Stark effect on electromagnetically induced transparency, *Phys. Rev. A* **60**, 2540 (1999).
- [50] M. D. Eisaman, A. André, F. Massou, M. Fleischhauer, A. S. Zibrov, and M. D. Lukin, Electromagnetically induced transparency with tunable single-photon pulses, *Nature* **438**, 837 (2005).
- [51] X. Xu, B. Sun, P. R. Berman, D. G. Steel, A. S. Bracker, D. Gammon, and L. J. Sham, Coherent population trapping of an electron spin in a single negatively charged quantum dot, *Nat. Phys.* **4**, 692 (2008).

- [52] R. W. Boyd, *Nonlinear Optics* (Elsevier Inc., 2008).
- [53] M. Mücke, E. Figueroa, J. Bochmann, C. Hahn, K. Murr, S. Ritter, C. J. Villas-Boas, and G. Rempe, Electromagnetically induced transparency with single atoms in a cavity, *Nature* **465**, 755 (2010).
- [54] J. R. Kuklinski, U. Gaubatz, F. T. Hioe, and K. Bergmann, Adiabatic population transfer in a three-level system driven by delayed laser pulses, *Phys. Rev. A* **40**, 6741 (1989).
- [55] K. Bergmann, H. Theuer, and B. W. Shore, Coherent population transfer among quantum states of atoms and molecules, *Rev. Mod. Phys.* **70**, 1003 (1998).
- [56] T. Takekoshi, L. Reichsöllner, A. Schindewolf, J. M. Hutson, C. R. Le Sueur, O. Dulieu, F. Ferlaino, R. Grimm, and H.-C. Nägerl, Ultracold dense samples of dipolar rbcbs molecules in the rovibrational and hyperfine ground state, *Phys. Rev. Lett.* **113**, 205301 (2014).
- [57] P. K. Molony, P. D. Gregory, Z. Ji, B. Lu, M. P. Köppinger, C. R. Le Sueur, C. L. Blackley, J. M. Hutson, and S. L. Cornish, Creation of ultracold $^{87}\text{Rb}^{133}\text{Cs}$ molecules in the rovibrational ground state, *Phys. Rev. Lett.* **113**, 255301 (2014).
- [58] K. S. Kumar, A. Vepsäläinen, S. Danilin, and G. S. Paraoanu, Stimulated Raman adiabatic passage in a three-level superconducting circuit, *Nat. Commun.* **7**, 10628 (2016).
- [59] N. V. Vitanov, A. A. Rangelov, B. W. Shore, and K. Bergmann, Stimulated Raman adiabatic passage in physics, chemistry, and beyond, *Rev. Mod. Phys.* **89**, 015006 (2017).
- [60] Z. Shi, C. B. Simmons, J. R. Prance, J. K. Gamble, T. S. Koh, Y.-P. Shim, X. Hu, D. E. Savage, M. G. Lagally, M. A. Eriksson, M. Friesen, and S. N. Coppersmith, Fast Hybrid Silicon Double-Quantum-Dot Qubit, *Phys. Rev. Lett.* **108**, 140503 (2012).
- [61] D. Kim, Z. Shi, C. B. Simmons, D. R. Ward, J. R. Prance, T. S. Koh, J. K. Gamble, D. E. Savage, M. G. Lagally, M. Friesen, S. N. Coppersmith, and M. A. Eriksson, Quantum control and process tomography of a semiconductor quantum dot hybrid qubit, *Nature* **511**, 70 (2014).
- [62] Z. Shi, C. B. Simmons, D. R. Ward, J. R. Prance, X. Wu, T. S. Koh, J. K. Gamble, D. E. Savage, M. G. Lagally, M. Friesen, S. N. Coppersmith, and M. A. Eriksson, Fast coherent manipulation of three-electron states in a double quantum dot, *Nat. Commun.* **5**, 1 (2014).
- [63] G. Cao, H.-O. Li, G.-D. Yu, B.-C. Wang, B.-B. Chen, X.-X. Song, M. Xiao, G.-C. Guo, H.-W. Jiang, X. Hu, and G.-P. Guo, Tunable Hybrid Qubit in a GaAs Double Quantum Dot, *Phys. Rev. Lett.* **116**, 086801 (2016).
- [64] D. P. DiVincenzo, D. Bacon, J. Kempe, G. Burkard, and K. B. Whaley, Universal Quantum Computation with the Exchange Interaction, *Nature* **408**, 339 (2000).
- [65] J. H. Shirley, Solution of the Schrödinger Equation with a Hamiltonian Periodic in Time, *Phys. Rev.* **138**, B979 (1965).
- [66] R. Winkler, *New York*, Springer Tracts in Modern Physics, Vol. 191 (Springer Berlin Heidelberg, Berlin, Heidelberg, 2003) p. 228.
- [67] J. R. Petta, A. C. Johnson, J. M. Taylor, E. A. Laird, A. Yacoby, M. D. Lukin, C. M. Marcus, M. P. Hanson, and A. C. Gossard, Coherent Manipulation of Coupled Electron Spins in Semiconductor Quantum Dots, *Science* **309**, 2180 (2005).
- [68] M. Pioro-Ladrière, T. Obata, Y. Tokura, Y. S. Shin, T. Kubo, K. Yoshida, T. Taniyama, and S. Tarucha, Electrically driven single-electron spin resonance in a slanting Zeeman field, *Nat. Phys.* **4**, 776 (2008).
- [69] S. Foletti, H. Bluhm, D. Mahalu, V. Umansky, and A. Yacoby, Universal quantum control of two-electron spin quantum bits using dynamic nuclear polarization, *Nat. Phys.* **5**, 903 (2009).
- [70] N. W. Hendrickx, D. P. Franke, A. Sammak, G. Scappucci, and M. Veldhorst, Fast two-qubit logic with holes in germanium, *Nature* **577**, 487 (2020).
- [71] K. Takeda, A. Noiri, J. Yoneda, T. Nakajima, and S. Tarucha, Resonantly Driven Singlet-Triplet Spin Qubit in Silicon, *Phys. Rev. Lett.* **124**, 117701 (2020).
- [72] S. Ashhab, J. R. Johansson, A. M. Zagorin, and F. Nori, Two-level systems driven by large-amplitude fields, *Phys. Rev. A* **75**, 063414 (2007).
- [73] J. Stehlik, M. D. Schroer, M. Z. Maialle, M. H. Degani, and J. R. Petta, Extreme Harmonic Generation in Electrically Driven Spin Resonance, *Phys. Rev. Lett.* **112**, 227601 (2014).
- [74] D. M. Zajac, A. J. Sigillito, M. Russ, F. Borjans, J. M. Taylor, G. Burkard, and J. R. Petta, Resonantly driven CNOT gate for electron spins, *Science* **359**, 439 (2018).
- [75] S. Oh, Y. P. Shim, J. Fei, M. Friesen, and X. Hu, Resonant adiabatic passage with three qubits, *Phys. Rev. A* **87**, 1 (2013).
- [76] Y. P. Kandel, H. Qiao, S. Fallahi, G. C. Gardner, M. J. Manfra, and J. M. Nichol, Adiabatic quantum state transfer in a semiconductor quantum-dot spin chain, *Nat. Commun.* **12**, 1 (2021).
- [77] S. Kohler, T. Dittrich, and P. Hänggi, Floquet-markovian description of the parametrically driven, dissipative harmonic quantum oscillator, *Phys. Rev. E* **55**, 300 (1997).